Organic Electronics 13 (2012) 623–631

Contents lists available at SciVerse ScienceDirect

Organic Electronics

journal homepage: www.elsevier.com/locate/orgel

Probing the effect of substrate heating during deposition of DCV4T:C_{60} blend layers for organic solar cells

Christian Koerner [a,*], Chris Elschner [a], Nichole Cates Miller [b], Roland Fitzner [c], Franz Selzer [a], Egon Reinold [c], Peter Bäuerle [c], Michael F. Toney [d], Michael D. McGehee [d], Karl Leo [a], Moritz Riede [a]

[a] Institut für Angewandte Photophysik, Technische Universität Dresden, George-Bähr-Straβe 1, 01062 Dresden, Germany
[b] Department of Materials Science and Engineering, Stanford University, Stanford, CA 94305, USA
[c] Institute of Organic Chemistry II and Advanced Materials, University of Ulm, Albert-Einstein-Allee 11, 89081 Ulm, Germany
[d] Stanford Synchrotron Radiation Lightsource, SLAC National Accelerator Laboratory, Menlo Park, CA 94025, USA

ARTICLE INFO

Article history:
Received 23 September 2011
Received in revised form 15 December 2011
Accepted 28 December 2011
Available online 13 January 2012

Keywords:
Morphology
Oligothiophene
Substrate heating
Organic solar cells

ABSTRACT

We present a comprehensive investigation of morphological changes inside the active layer of an organic solar cell induced by substrate heating during layer deposition by thermal evaporation in ultra-high vacuum. To explore the trends observed in solar cell devices, we apply absorption and photoluminescence spectroscopy, atomic force microscopy, X-ray diffraction, and organic field effect transistor measurements. The material combination we use comprises unsubstituted dicyanovinyl end-capped quaterthiophene (DCV4T) as the donor material mixed with C_{60} as the acceptor. The solar cell power conversion efficiency decreases with increasing substrate temperature during film deposition due to changes in the crystalline structure of the oligothiophene phase, leading to a decrease in absorption strength. Photoluminescence measurements show that substrate heating increases the amount of phase separation between the donor and acceptor, and topology and structure investigations reveal large aggregates of polycrystalline DCV4T at the surface. However, the fill factor is increased for higher substrate temperatures due to better transport properties. The highest efficiency obtained with this material combination and stack design is 3.0% under AM1.5g illumination.

1. Introduction

Power conversion efficiencies (PCE) of organic solar cells (OSC) have increased significantly in the last several years, reaching 8.3% for polymer-based [1] as well as small-molecule-based [2] systems. The most efficient organic solar cells are based on a bulk heterojunction architecture, which ideally contains a continuous, interpenetrating network of a donor (D) and an acceptor (A) material. If the D and A are mixed too finely, many of the charge carriers will not have continuous pathways to their respective electrodes and therefore will not contribute to the solar cell current. On the other hand, if the D–A phase separation is too large, many of the excitons will recombine prior to reaching a D–A interface, where they can be split into free charges. Thus, there is a trade-off between exciton splitting (charge generation) and charge transport.

In the field of polymer OSC, there are many ways to influence the nano-scale morphology in a D–A blend layer, e.g. thermal annealing [3,4], solvent annealing [5], or the use of different solvents [6] or solvent additives [7–9]. For devices using small molecules, which are usually thermally evaporated in an ultra-high vacuum (UHV) chamber, the most successful technique to alter the morphology is the deposition of the active layer onto heated substrates [10,11]. Pfuetzner et al. [12] showed that they can double the power conversion efficiency of devices using ZnPc

* Corresponding author. Tel.: +49 0351 46335117.
E-mail address: christian.koerner@iapp.de (C. Koerner).

1566-1199/$ - see front matter © 2012 Elsevier B.V. All rights reserved.
doi:10.1016/j.orgel.2011.12.017

and C_{60} as active layer by heating the substrate during film deposition. They attributed this efficiency increase to an increase in the hole mobility of ZnPc by one order of magnitude and to better percolation pathways in the blend film resulting in high short-circuit current densities (j_{sc}) and fill factors (FF). In a similar investigation Wynands et al. [13] showed that they were able to tune the blend morphology of dicyanovinyl end-capped sexithiophene thin films to obtain efficient exciton splitting, high current densities and good transport properties by optimizing the substrate temperature during evaporation of the active layer.

In this paper, we investigate another oligothiophene derivative, the unsubstituted dicyanovinyl end-capped quaterthiophene (DCV4T) (see Fig. 1). Fitzner et al. [14] reported flat heterojunction solar cells using this material as donor with an efficiency of 1.2% and a high V_{oc} of 0.97 V. However, the current density was low due to the very thin absorber layer (6 nm). Here, we show that this material can give up to 3.0% PCE in a bulk heterojunction (BHJ) architecture. However, with increasing temperature it shows a completely different behavior than observed by Wynands et al. for the sexithiophene derivative. These quaterthiophene molecules have a very high tendency to form macroscopic aggregates, which are detrimental to exciton splitting. Beyond that, the crystal orientation within these aggregates is unfavorable for absorption, which further decreases the PCE of such devices. Thus, substrate heating is not always beneficial for OSC device performance, but strongly depends on the packing of donor and acceptor in the active layer.

We show the influence of substrate heating during layer deposition on solar cell devices incorporating mixed layers of DCV4T (D) with C_{60} (A) as active layer. Therefore, we investigated the thin film morphology of DCV4T:C_{60} blend films deposited at various substrate temperatures by means of atomic force microscopy (AFM) and X-ray diffraction (XRD) and monitored the changes in absorption and photoluminescence (PL) of these layers. We complement our results with mobility measurements using organic field-effect transistors (OFET).

2. Experimental

DCV4T was synthesized as described in [14]. The material was purified by gradient vacuum sublimation prior to use. C_{60} (Bucky, USA) was purified twice by gradient vacuum sublimation. Glass substrates coated with indium tin oxide (ITO, Thin Film Devices, USA) with a sheet resistance of 30 Ω/□ were used as a transparent electrode for the solar cell devices. The mixed layers were prepared by co-evaporation in an UHV chamber with a base pressure of better than 10^{-8} mbar. The different substrate temperatures T_{sub} during evaporation were realized by resistive heating for temperatures higher than room temperature and by contact cooling with liquid nitrogen for the cooled sample. The following stack design was used for the solar cell devices: ITO/C_{60} (15 nm)/DCV4T:C_{60} (20 nm, 2:1 by volume, substrate at T_{sub})/i-HTM (5 nm)/p-HTM (50 nm)/p-dopand (1 nm)/Au (50 nm). As hole transporting material (HTM), we used BPAPF (9,9-bis[4-(N,N-bis-biphenyl-4-yl-amino)phenyl]-9H-fluorene, Lumtec, Taiwan) p-doped with NDP9 (Novaled AG, Germany). The layer thicknesses during deposition were monitored using quartz oscillators and density values of 1.54 g/cm^3 for C_{60}, 1.37 g/cm^3 for DCV4T and 1.2 g/cm^3 for BPAPF. All solar cells were encapsulated in a nitrogen atmosphere without air contact and measured at room temperature under an AM1.5g sun simulator SC1200 (KHS Technical Lighting, Germany) at approximately 100 mW/cm^2 after mismatch correction. All devices had an area of about 6 mm^2, as determined by a second j–V measurement using a shadow mask with a fixed aperture of 2.958 mm^2. More details about the measurement setup for j–V characteristics and EQE can be found in Ref. [13].

For absorption, PL and AFM measurements, we used the same stack as for the solar cells except for the hole transport layer and the metal. Bare glass and quartz glass were used as a substrate, respectively. For transmission (T) and reflection (R) measurements, we used a PerkinElmer lambda900 spectrometer. The absorption (A) was calculated using $A = 1 - R - T$ (neglecting thin film effects from the substrate). For PL measurements, all samples were excited with a xenon arc lamp at 550 nm and measured with a Edinburgh Instruments FSP920 fluorescence spectrometer. A Nanoscope III AFM in tapping mode was used for the topography measurements.

For the XRD measurements, the samples were produced by evaporation in a different vacuum chamber with a base pressure of $p \leqslant 10^{-6}$ mbar. Some of the samples were pre-

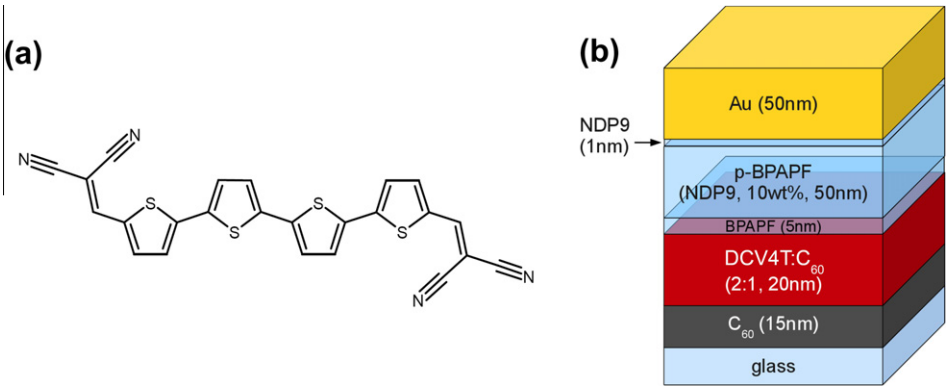

Fig. 1. (color online) (a) Molecular structure of DCV4T. (b) Solar cell device stack used within this work as described in the experimental section.

pared with 1:1 molar ratio instead of volume mixing used for the solar cells. However, a comparison of XRD pattern from 1:1-mol. and 1:1-vol. blend layers showed no significant differences.

Grazing incidence X-ray diffraction (GIXRD) measurements are carried out on a Bruker AXS D8 Discover. As beam optics a Göbel mirror and Cu Kα radiation in combination with a scintillation detector is used. For comparison, 2D GIXRD measurements were performed using a Mar2300 image-plate detector at beamline 11-3 at the Stanford Synchrotron Radiation Lightsource at an energy of 12,735 eV and an incidence angle of 0.12°.

3. Results

3.1. Solar cells

First, we prepared four identical BHJ solar cells with the active layer (DCV4T:C_{60}, 2:1 by volume) evaporated at different substrate temperatures between 30 and 90 °C (stack details are shown in Fig. 1b). The resulting current–voltage (j–V) characteristics can be seen in Fig. 2. The device evaporated on a room temperature substrate shows good performance with $j_{sc} = 6.49$ mA/cm^2, an open-circuit voltage (V_{oc}) of 0.98 V, and a *FF* of 48.4%. This results in a mismatch corrected PCE of 3.0%. Photoinduced absorption measurements indicate that the current density may be limited by recombination of the excited charge transfer state to the donor triplet state, which can hardly be dissociated and thus cannot contribute to the photocurrent. The *FF* is limited by both the unfavorable small scale morphology of the blend layer and an injection barrier between DCV4T and the hole transporting layer, because the HOMO levels of the materials are not perfectly aligned.

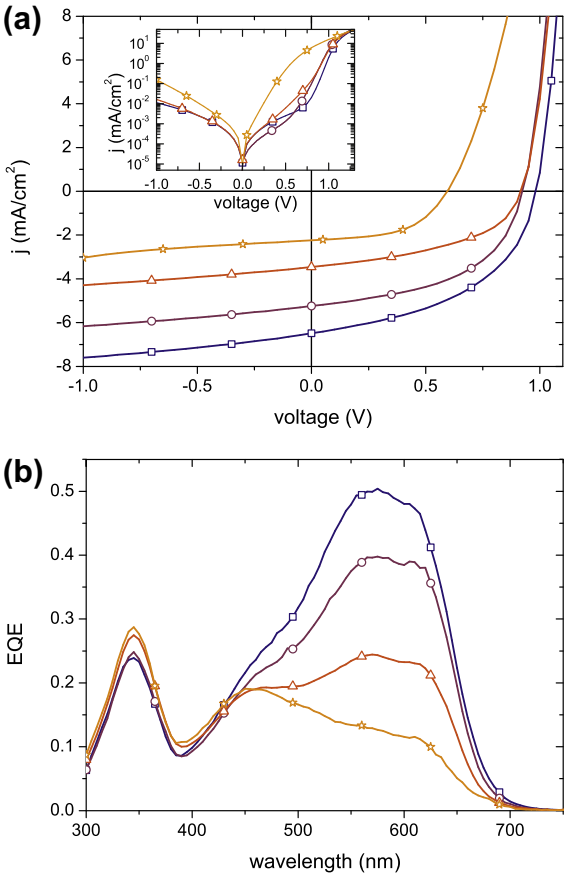

Fig. 2. (color online) (a) j–V characteristics and (b) EQE for DCV4T:C_{60} BHJ solar cells with the active blend layer deposited at different substrate temperatures: 30 °C (blue, squares), 50 °C (violet, circles), 70 °C (red, triangles) and 90 °C (orange, stars). The inset to (a) shows the j–V characteristics in dark displayed on a lin-log scale. The solar cell device stack is shown in Fig. 1. The EQE data is used to calculate the mismatch factor for device characterization.

Upon increasing the substrate temperature during evaporation of the active layer, the performance decreases: At 90 °C, j_{sc} and V_{oc} decrease to 2.24 mA/cm^2 and 0.6 V, respectively. The *FF* slightly increases to 53%, which could be attributed to better transport in the highly crystalline DCV4T. The inset to Fig. 2 shows the j–V characteristics in the dark on a lin-log scale. The current density in reverse bias increases at 90 °C substrate temperature. This bad diode blocking behavior occurs due to shunts caused by increased roughness of the active layer as will be shown later by AFM measurements. The solar cell parameters extracted from the measurements are listed in Table 1. The saturation value S is a measure of the field dependence of charge carrier collection and the diode character of the device and is defined as $S = j(-1V)/j(0V)$.

External quantum efficiency (EQE) measurements show the best performance for the device prepared on 30 °C substrates with a maximum EQE of 50% (Fig. 2). The EQE drops for higher substrate temperatures. However, for higher temperatures an increase in the vibronic substructure of the thiophene absorption is visible which will be discussed below. It can also be seen that the decrease in current is only due to a decrease in the thiophene absorption region whereas the current output from C_{60} even slightly increases with substrate temperature.

We will show that morphological changes in the active layer due to deposition on a heated substrate can explain this behavior.

3.2. Absorption and photoluminescence

Absorption measurements can be used to track macroscopical morphological changes in the active layer. We therefore prepared samples with the active layer deposited at the same substrate temperatures as used for the solar

Table 1
Solar cell parameters for the mixed heterojunction solar cells with the active layer deposited at different substrate temperatures T_{sub}. In addition to the characteristic solar cell parameters j_{sc}, V_{oc}, *FF* and *PCE* the saturation value S, the mismatch corrected incident light intensity I_L and the pixel area A are given.

T_{sub} (°C)	j_{sc} (mA/cm^2)	V_{oc} (V)	*FF* (%)	S	*PCE* (%)	I_L (mW/cm^2)	A (mm^2)
30	6.49	0.98	48.4	1.17	3.0	102	5.71
50	5.24	0.92	51.0	1.18	2.4	102	5.26
70	3.46	0.92	47.0	1.24	1.5	102	5.79
90	2.24	0.60	52.9	1.35	0.71	100	5.97

cell devices shown above. To mimic real solar cell conditions, all these layers were produced on top of a 15 nm C_{60} sublayer. The absorption A was calculated from the measured transmission T and reflection R using $A = 1 - R - T$. All measurements were performed in ambient conditions.

The absorption due to the DCV4T decreases with increasing substrate temperature (Fig. 3). This decrease is one of the reasons for the j_{sc} decrease we observe. The mechanism behind this decrease in absorption is still under debate. However, our XRD results (Fig. 9) indicate that the orientation of the molecular crystals changes by heating the substrate during evaporation. It is known that the absorption is low if the long axis of the molecule is parallel to the light-propagation direction [15]. Such a rearrangement could thus be responsible for the described decrease in absorption. From photoluminescence measurements, we can exclude chemical degradation of the molecule as the emission spectrum does not change. Moreover, the substrate-temperature range during deposition is well below the evaporation temperature of the material and should therefore not harm the molecules.

Furthermore, the vibronic substructure in the region where the DCV4T absorbs strongly becomes more pronounced. Above 50 °C, three vibronic modes are clearly visible. The appearance of vibronic peaks is often interpreted as increased molecular ordering [8,16] due to crystallization [17] in the thin films or an increase in the planarity of the molecules [18]. At 90 °C, the spectrum is very similar to the neat layer absorption spectrum of DCV4T, which is represented by the black line in Fig. 3 indicating that the donor phases must be large enough to restore the undisturbed crystalline neat layer morphology. Another noticeable change appears at higher wavelengths where an additional feature shows up for the 70 °C and 90 °C samples. These features persist out to 900 nm, where the molecules do not absorb. The EQE does not show any contribution to the photocurrent in this spectral region. Therefore, we attribute this to scattered light in the sample, which causes an underestimation of the transmission (and thereby an overestimation of absorption) since only direct transmission was considered in our experiment. The amount of scattered light increases with substrate temperature and can be due to an increase in the roughness of the deposited layer, which we will show by AFM measurements. The same increase in absorption can be seen at 350 and 450 nm. However, contrary to the scattering causing the mentioned virtual absorption at higher wavelengths, it does increase the real absorption in the active layer due to the extended light path inside the active layer as evident from the small increase in the EQE at 350 nm (Fig. 2).

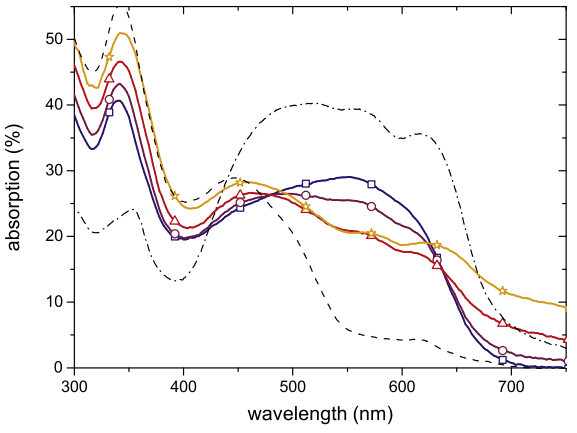

Fig. 3. (color online) Absorption spectra of DCV4T:C_{60} mixed layers (20 nm, 2:1 by volume) deposited on top of a 15 nm C_{60} sublayer at different substrate temperatures: 30 °C (blue, squares), 50 °C (violet, circles), 70 °C (red, triangles) and 90 °C (orange, stars). For comparison, the absorption spectra of 30 nm thick neat layers of C_{60} (dashed) and DCV4T (dash-dot), respectively, are shown in black.

A deeper insight into the microscopic blend structure can be gained by photoluminescence (PL) measurements. Generally, mixing only a small amount of an acceptor into a donor matrix (assuming appropriate energy levels) leads to very efficient quenching of the donor luminescence. This is due to very fast and efficient charge transfer from the donor to the acceptor leading to the formation of charge transfer (CT) states at the D–A interface. For this charge transfer to happen, the excitons have to reach the interface within their lifetime, which is generally quite short (between ps and ns). Combined with the low mobility in organic materials, this leads to exciton diffusion lengths between 5 and 20 nm for most organic materials [19]. If the mixing of donor and acceptor is very intimate (no phase separation), every exciton should be able to reach the interface. The luminescence of the donor is thus fully quenched and a new red shifted emission band arises originating from luminescent decay of CT states [20–23]. However, if the molecules aggregate in separate phases (strong phase separation), some excitons will no longer be able to reach the interface and will consequently recombine by giving off luminescence from the pure donor component. Hence, PL measurements provide insight into changes in the phase separation between the donor and the acceptor.

The measured spectra show significant changes on increasing substrate temperature (see Fig. 4). At 30 °C, the luminescence is strongly quenched compared to the neat layer luminescence (not shown). A new shoulder shows up at higher wavelengths which can be attributed to emission from a CT state. We conclude that the mixing behavior of DCV4T and C_{60} is very good at substrate temperatures of 30 °C and the phase size is less than 10 nm. At higher temperatures the emission at 666 nm increases by more than a factor of 40 and the spectral shape changes, indicating demixing of donor and acceptor. Moreover, at a substrate temperature of 90 °C, CT luminescence is no longer visible. The reason for this could be a strong demixing of donor and acceptor, an increase in CT state dissociation (less luminescent geminate recombination) or simply the fluorescence of the thiophene excitons being much stronger. The increase in PL partially explains the loss in j_{sc} because the excitons that recombine cannot contribute to the photocurrent.

3.3. Atomic force microscopy (AFM)

In general, it is difficult to interpret the surface topography measured by AFM in terms of phase separation be-

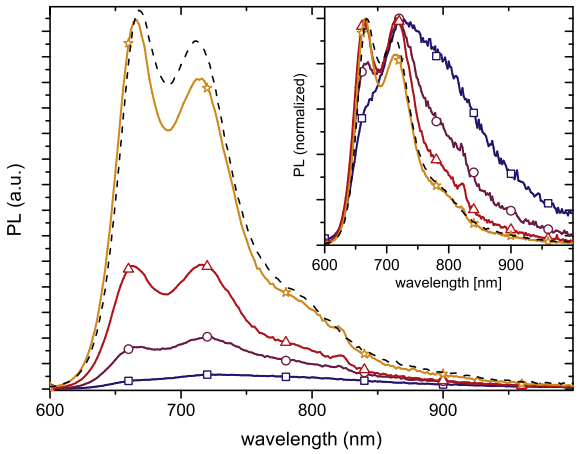

Fig. 4. (color online) Photoluminescence spectra of DCV4T:C_{60} mixed layers (20 nm, 2:1) deposited on top of a 15 nm C_{60} sublayer at different substrate temperatures: 30 °C (blue, squares), 50 °C (violet, circles), 70 °C (red, triangles) and 90 °C (orange, stars). The dashed black line shows the photoluminescence of a sample consisting of C_{60} (15 nm)/C_{60} (6.7 nm, 90 °C)/DCV4T (13.3 nm, 90 °C). The inset shows all PL spectra normalized to their respective maximum.

cause the technique itself is not sensitive to chemical differences. However, macroscopic changes in the morphology and maybe even crystallinity of the sample should also be reflected by the surface topography and roughness.

The measured $5 \times 5\ \mu m^2$ topography images can be seen in Fig. 5. All images show curved worm-like structures at the surface with length scales of more than 1 μm and thicknesses of 100–200 nm. The maximum peak heights reach higher than 100 nm even though the overall deposited nominal blend layer thickness was only 20 nm. The maximum scale displayed in the figure increases with substrate temperature. The root mean square (*rms*) roughness values extracted from Fig. 5 also increase from 13 to 25 nm. These measurements confirm the assumption of high roughness causing the strong scattering seen in the absorption measurements.

As previously mentioned, it is not possible to distinguish between DCV4T and C_{60} only from the topography images. However, we could at first draw the assumption that these worm-like structures represent pure oligothiophene aggregates. As these aggregates are even present for the sample prepared at $T_{sub} = 30$ °C, this would either contradict the strong PL quenching or demand that the major part of the donor molecules is still mixed with C_{60} in the bulk of the layer, where exciton quenching can take place. In contrast to this, at 90 °C the oligothiophene PL increased strongly and a large phase separation was suggested. This matches well the results from AFM measurements assuming that most of the oligothiophene molecules are aggregated in these structures. To verify these findings, we estimate the volume of the surface structures in Fig. 5 and compare the values with the total volume of deposited DCV4T. To do this, we make the simplified assumption that the structures do not extend into the rest of the bulk layer underneath. The results of these calculations are shown in Table 2. For the sample prepared on a 30 °C substrate the ratio between evaporated DCV4T volume and the masked structure volume is only 20%. In comparison, this value in-

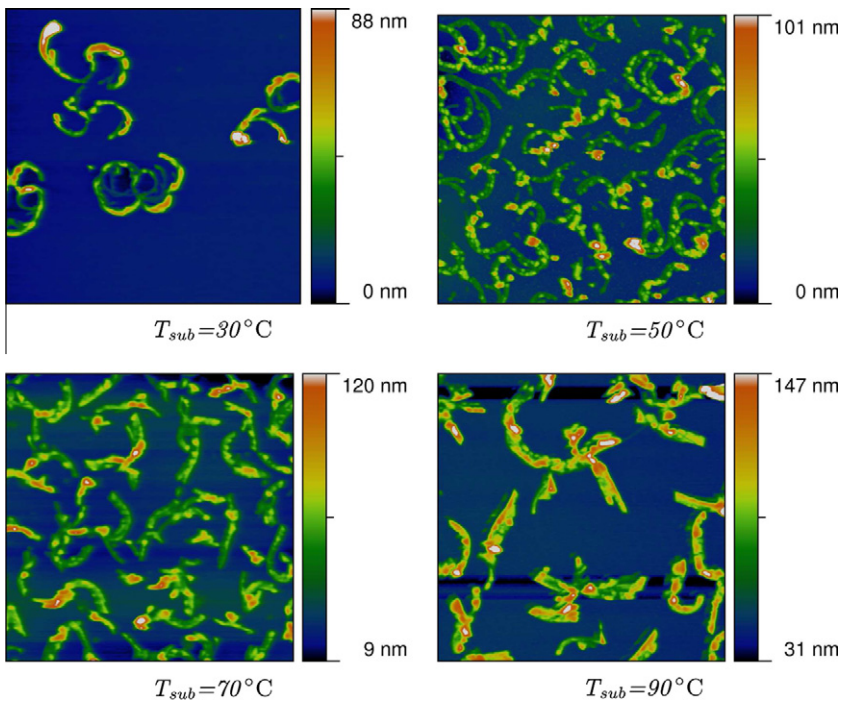

Fig. 5. (color online) AFM topography images taken on top of the DCV4T:C_{60} blend layer which was deposited at different substrate temperatures T_{sub}. The size of all images is $5 \times 5\ \mu m^2$.

Table 2
Calculated volume of the structures visible in the AFM images compared to the volume of deposited DCV4T. For the expected volume, a thickness of 13.3 nm had been assumed. T_{sub} is the substrate temperature during evaporation of the blend layer. The statistical error between two images at different sample positions is below 20%.

T_{sub} (°C)	Image size (μm^2)	Calc. vol. (μm^3)	Expect. vol. (μm^3)	Ratio (%)
30	5 × 5	0.078	0.333	23
50	5 × 5	0.158	0.333	47
	2.5 × 2.5	0.044	0.083	53
70	5 × 5	0.253	0.333	76
	2 × 2	0.036	0.053	68
90	5 × 5	0.289	0.333	87

creases to nearly 90% when the blend layer is deposited on a 90 °C substrate.

Thus, we suggest that the blend morphology for these layers resembles the illustrations in Fig. 6. At low substrate temperatures, most of the material is well mixed and the phase separation is small. At the surface, pure DCV4T aggregates form. At higher substrate temperatures, the donor and acceptor phases demix. The major part of the thiophene volume contributes to the surface aggregations, increasing their size and the surface roughness.

3.4. X-ray investigations

3.4.1. GIXRD measurements

Using X-ray diffraction, we can study the crystalline regions in the films. Thus, it allows to monitor morphological changes in the active layer induced by the deposition on heated substrates. All thin film samples are measured with a GIXRD (grazing incidence X-ray diffraction) setup. A detailed description of the measurement conditions is given in [24].

In the following, we present XRD structure investigations to strengthen the proposed picture by selectively probing the crystallinity in the bulk and at the surface of the samples.

The GIXRD measurements are presented in Fig. 7. The room-temperature sample shows a high amount of diffuse scattering between 1.2 and 2 $Å^{-1}$, indicating a high degree of disorder in the blend layer. There are no Bragg reflections that can be clearly identified with DCV4T. From the broadened $C_{60}(1\,1\,1)$ Bragg reflection at $Q = 0.75\ Å^{-1}$, we can deduce the crystal size of C_{60} using the Scherrer equation to ≈3 nm. Thus, the room temperature sample only contains nanocrystalline C_{60} and amorphous DCV4T. When the sample is prepared on a heated substrate ($T_{sub} = 90$ °C), several Bragg reflections of C_{60} and DCV4T show up at the same positions as in single layers, indicating an increase in the phase separation, which allows the donor and acceptor materials to pack in their respective crystalline phases (for details about C_{60} single phases cf. Ref. [24]). The C_{60} crystals grow in size to 8 nm, which can be seen from the sharpening of the $C_{60}(1\,1\,1)$ reflection. The new Bragg reflection at $Q = 0.907\ Å^{-1}$ can be clearly assigned to DCV4T, as the angular position fits very well to measurements on neat DCV4T films. This Bragg-reflection is correlated to a lattice spacing of $d = 6.91$ Å which is much shorter than the long axis of DCV4T (≈22 Å). Although we do not know the exact positions of the molecules in the unit cell, we can at least be sure that they are not standing upright on the substrate but rather lying edge-on or face-on. From the peak width, we can deduce the DCV4T crystal size of approximately 14 nm in the mixed layer. The heated sample shows no diffuse scattering, which suggests that the crystalline phases are dominant in the heated blend layer. The fact that we see different crystal orientations for C_{60} ((1 1 1), (2 2 0), (3 1 1)) shows that C_{60} grows polycrystalline with randomized orientation while the DCV4T crystals grow with a preferred orientation in the heated blend layer. We expect that this is due to the high symmetry of C_{60}.

Combining the AFM and GIXRD measurements could lead to the conclusion that – at least for the sample prepared on the 30 °C substrate – the surface structures in Fig. 5 contain only amorphous material. Still, if these structures only consist of oligothiophene molecules, it is very unlikely that they form these aggregates without packing in their crystalline phase. Although XRD usually probes the morphology in the bulk of the sample and is not very surface sensitive, but varying the X-ray incidence angle allows some control over the X-ray probing depth of the film. In order to directly gather diffraction information from the surface, the incident angle has to be smaller than the critical angle of total reflection of the organic blend layer. A comparison between the bulk-sensitive and the surface-sensitive measurements for the sample prepared at room temperature is shown in Fig. 8. Both diffraction patterns

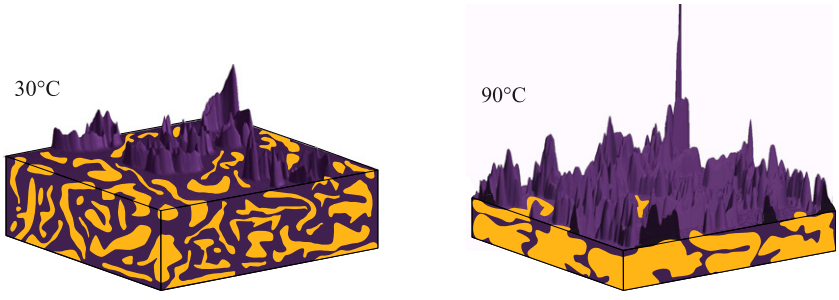

Fig. 6. (color online) Sketch of the proposed morphology picture of DCV4T:C_{60} blend layers deposited at substrate temperatures of 30 °C and 90 °C. Purple parts represent the DCV4T phase, yellow parts represent C_{60} phase. For the surface, 3D images of the AFM measurements in Fig. 5 were used. The pictures are not drawn to scale and should be considered as idealized visualization of the morphology change induced by substrate heating during evaporation.

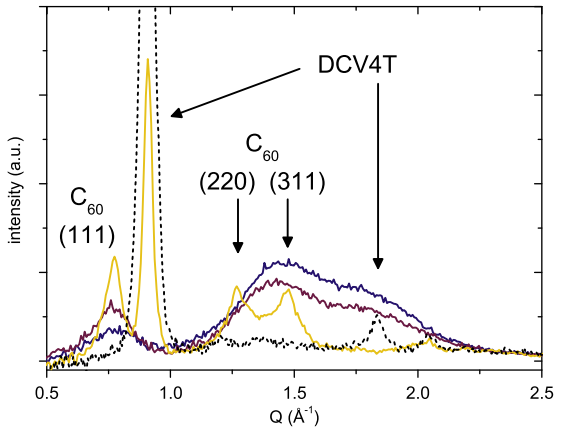

Fig. 7. (color online) GIXRD measurements of DCV4T:C_{60} blend layers (1:1 molar ratio) deposited onto a glass substrate at different substrate temperatures: 30 °C (blue) and 90 °C (orange). The layer thickness was 100 nm for every sample. The dashed black line shows the GIXRD measurement on a 50 nm thick single layer of DCV4T.

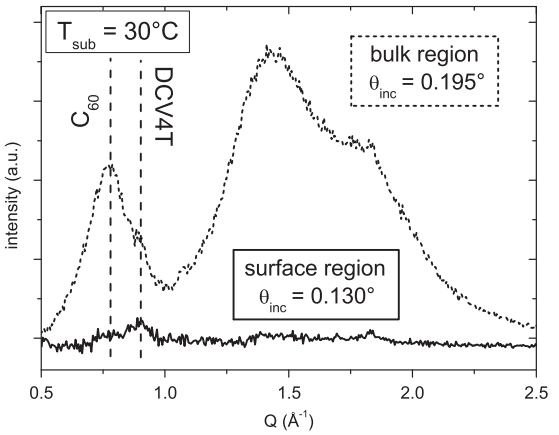

Fig. 8. Comparison between diffraction information from the bulk of the organic blend layer and the surface. Θ_{inc} is the angle of incidence for X-ray radiation. The sample consists of a 200 nm DCV4T:C_{60} blend layer (1:1 by volume) deposited onto a glass substrate at 30 °C.

are background corrected with an exponential fit. The diffraction pattern of the bulk region is nearly identical to the result shown in Fig. 7, although mixing ratio and film thickness of the samples are slightly different. The bulk measurement shows again the nanocrystalline C_{60} and amorphous DCV4T behavior in the film. On the other hand, the surface measurement shows a weak DCV4T Bragg reflection. The surface measurement intensities are as expected much lower than the bulk intensities due to the lower scattering volume. However, the relative intensities of the DCV4T and C_{60} reflections are quite different for the bulk and the surface measurement showing that the ratio between crystalline DCV4T and crystalline C_{60} is much higher at the surface compared to the bulk. Hence, this GIXRD-surface measurement gives more evidence of the proposed assumption that the surface structures, which are visible in the AFM measurements, are polycrystalline DCV4T aggregates either lying on top of or protruding from an amorphous DCV4T:C_{60} blend layer.

3.4.2. 2D GIXRD measurements

All GIXRD measurements are carried out on relatively large film thickness samples to get high diffraction intensities. To compare these findings with thinner films with thicknesses similar to those used in solar cells, further investigations at the Stanford Synchrotron Radiation Lightsource were done. The result of these measurements is shown in Fig. 9. The measurement can be compared to those presented in Figs. 7 and 8 by looking in Q_z direction at $Q_{xy} = 0$, which represents the out-of-plane scattering direction. The in-plane scattering (along Q_{xy} in Fig. 9) gives information about crystallinity parallel to the surface.

The 30 °C sample shows weak Bragg reflections from C_{60}(1 1 1) and the known DCV4T reflection at $Q = 0.907$ Å^{-1}. This is in opposite to the GIXRD measurement in Fig. 7 where no DCV4T reflection was present at the 30 °C sample. However, the samples we used for the 2D GIXRD measurements were only 20 nm thick compared to 100 or 200 nm for the 1D GIXRD measurements. So, we assume that the 2D GIXRD measurement mixes bulk and surface related structure information, resolving also the DCV4T peak we had seen in the surface sensitive GIXRD measurement (Fig. 8).

Going to the 50 °C sample, we see a strong sharpening of the peaks indicating increased order due to heating the substrate during film deposition.

At $Q = 1.82$ Å^{-1} another reflection occurs which is also present in the DCV4T neat layer diffraction pattern (Fig. 7). This reflection may be correlated to a π–π-stacking

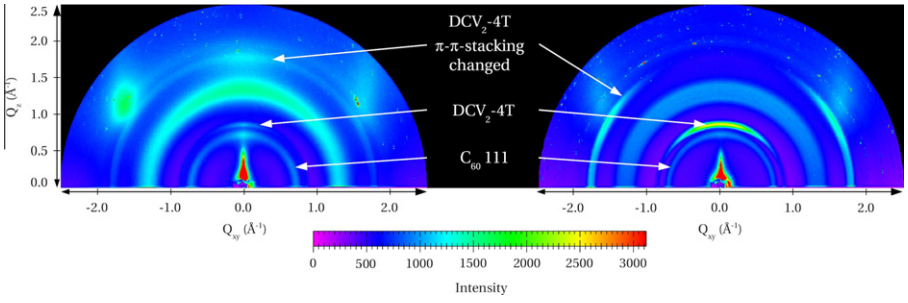

Fig. 9. (color online) 2D GIXRD measurement performed on 20 nm DCV4T:C_{60} blend layers (1:1 by volume) deposited onto a silicon substrate at substrate temperatures of 30 °C (left) and 50 °C (right), respectively.

Bragg reflection. The corresponding lattice spacing is $d = 3.45$ Å.

Interestingly, the orientation of this reflection changes with substrate temperature. For the 30 °C sample, both reflections ($Q = 0.907$ Å^{-1} and 1.82 Å^{-1}) peak in the Q_z direction and show only diffuse or no diffraction signal for higher angles in the Q_{xy}—Q_z-plane. This indicates that for either crystal direction, the out-of-plane stacking is preferred compared to the direction parallel to the substrate. The lack of significant in-plane reflections indicates a rather one-dimensional rod-like crystal growth in this sample. However, for the 50 °C sample the π–π-stacking peak shifts to the in-plane direction and the intensity of the reflection is increased. Moreover, as the reflection arcs at $Q = 0.907$ Å^{-1} and $Q = 1.82$ Å^{-1} do not overlap we can conclude that these reflections are representatives of different directions in the same crystal. Thus, the heated sample shows two-dimensional crystallinity with the π–π-stacking direction parallel to the surface. We assume that this structural change is the reason for the reduction of absorption strength, which was observed for the thin film evaporated onto high temperature substrates (Fig. 3).

Finally, the XRD results indicate that the crystallinity of both the C_{60} and the DCV4T are probably increasing. By surface sensitive GIXRD measurements we can confirm that already for preparation on unheated substrates there is a small amount of crystalline DCV4T at the surface whereas the bulk of the layer is amorphous which confirms our assumptions drawn from AFM measurements. Furthermore, the rearrangement of molecular crystals visible in 2D GIXRD measurements on thin layers could possibly explain the decrease in absorption at high substrate temperatures.

To confirm all these findings, two more experiments were performed that provide further evidence for the presented morphology picture. Field-effect transistors are widely used to measure the charge carrier mobility in organic materials. With this experiment, the lateral mobility parallel to the substrate can be measured. The 20 nm blend layer, which was deposited onto a 30 °C substrate, shows hole mobilities comparable to those in a pure DCV4T layer. This shows that DCV4T must form closed and highly interconnected percolation paths within the blend layer at least in lateral direction between the source and drain contacts. However, if the blend layer is deposited onto a 90 °C substrate, no hole conduction is observed. According to the AFM measurements, close to 100% of the DCV4T molecules aggregate at the surface without any interconnection. Therefore, the holes cannot travel from source to drain and no lateral current can be measured. However, due to the increased crystallinity shown by XRD measurements, the transport perpendicular to the substrate should improve which explains the increase in FF by deposition onto the heated substrate.

Secondly, the proposed morphology picture makes it clear that the heated blend layer looks rather like a bilayer structure. We would therefore expect the PL not to be significantly different from a bilayer structure with the same layer thicknesses both deposited at 90 °C. The result of this measurement is shown in Fig. 4. It is obvious that the PL of the subsequently deposited layers (black dashed line) coincides with the blend layer luminescence in spectral shape as well as emission strength.

As heating the substrate was not beneficial to the solar cells with DCV4T as donor material, we cooled the substrate to −30 °C during deposition of the blend layer to prevent the strong thiophene aggregation and provide a more intimate mixing between donor and acceptor. However, solar cell j–V and EQE measurements show that nearly all solar cell parameters are worse compared to the sample prepared at room temperature (not shown). Most significantly, the FF drops to nearly 30%. Probably, the reason for this decrease is the bad transport behavior in this too finely mixed blend layer. GIXRD measurements even show an increase in the amorphous part between 1.2 and 2 Å^{-1}, which is also dominant for the sample prepared at 30 °C substrate (see Fig. 7). Accordingly, the C_{60} nanocrystallite size decreases to around 2 nm, which would roughly correspond to a box of only $3 \times 3 \times 3$ molecules. Moreover, the PL is also strongly quenched, similar to the 30 °C sample. This shows that the blend layer deposited on a cooled substrate exhibits a high degree of disorder and small phases. However, in the surface sensitive GIXRD measurements, we can also see a Bragg-reflection at 0.907 Å^{-1} which was attributed before to crystalline DCV4T. This indicates that even if the substrate is cooled during deposition the DCV4T molecules still form aggregates at the surface, however presumably with smaller total volume compared to what we had seen for the other samples from AFM measurements.

3.5. Conclusion

We demonstrate that organic solar cells using a DCV4T:C_{60} blend layer as active photon-to-electron converting material combination do not benefit from substrate heating during deposition in contrast to other publications dealing with the deposition of small molecules onto heated substrates. The reason is a dramatic change in the blend layer morphology. The decrease in current on increasing substrate temperature is due to a strong phase separation of donor and acceptor. This phase separation prevents many of the excitons from reaching the D/A interface, causing them to recombine as evident from photoluminescence measurements. Additionally, the absorption decreases presumably due to an unfavorable alignment of the molecular dipole to the incoming light. A small increase in EQE in the C_{60} absorption region caused by scattered light due to the high blend layer roughness slightly moderates the current decrease. The roughness was validated by AFM measurements which revealed large crystalline DCV4T aggregates either lying on top of or protruding from the DCV4T:C_{60} bulk layer. The increase in FF can be attributed to better transport properties due to a higher degree of crystallinity upon heating. However, cooling did not increase solar cell efficiency because of weak transport properties due to a highly amorphous mixing of donor and acceptor. For this material combination and stack design, deposition of the DCV4T:C_{60} blend layer on 30 °C substrate temperature gives the highest efficiency of 3.0% under AM1.5g illumination.

Acknowledgements

We thank Moritz Hein and Jens Jankowski for the preparation, measurement, and evaluation of the OFET data, Dr. Lutz Wilde at Frauenhofer CNT for the GIXRD measurements. Parts of this research were carried out at the Stanford Synchrotron Radiation Lightsource, a national user facility operated by Stanford University on behalf of the US Department of Energy, Office of Basic Energy Sciences. The Deutsche Forschungsgemeinschaft (DFG) is acknowledged for funding within the Priority Program SPP 1355 as well as the German Federal Ministry of Education and Research (BMBF) within the OPA project (BMBF 13N9872).

References

[1] Konarka Technologies, Inc., Press release, 2010.
[2] Heliatek GmbH, Press release, 2010.
[3] F. Padinger, R. Rittberger, N. Sariciftci, Effects of postproduction treatment on plastic solar cells, Advanced Functional Materials 13 (2003) 85–88.
[4] W. Ma, C. Yang, X. Gong, K. Lee, A.J. Heeger, Thermally stable, efficient polymer solar cells with nanoscale control of the interpenetrating network morphology, Advanced Functional Materials 15 (2005) 1617–1622.
[5] G. Li, Y. Yao, H. Yang, V. Shrotriya, G. Yang, Y. Yang, Solvent annealing effect in polymer solar cells based on poly(3-hexylthiophene) and methanofullerenes, Advanced Functional Materials 17 (2007) 1636–1644.
[6] J. Liu, Y. Shi, Y. Yang, Solvation-induced morphology effects on the performance of polymer-based photovoltaic devices, Advanced Functional Materials 11 (2001) 420.
[7] F. Zhang, K. Jespersen, C. Björström, M. Svensson, M. Andersson, V. Sundström, K. Magnusson, E. Moons, a. Yartsev, O. Inganäs, Influence of solvent mixing on the morphology and performance of solar cells based on polyfluorene copolymer/fullerene blends, Advanced Functional Materials 16 (2006) 667–674.
[8] J. Peet, J.Y. Kim, N.E. Coates, W.L. Ma, D. Moses, A.J. Heeger, G.C. Bazan, Efficiency enhancement in low-bandgap polymer solar cells by processing with alkane dithiols, Nature Materials 6 (2007) 497–500.
[9] Y. Zhang, Z. Li, S. Wakim, S. Alem, S.-W. Tsang, J. Lu, J. Ding, Y. Tao, Bulk heterojunction solar cells based on a new low-band-gap polymer: morphology and performance, Organic Electronics 12 (2011) 1211–1215.
[10] K. Suemori, T. Miyata, M. Hiramoto, M. Yokoyama, Enhanced photovoltaic performance in fullerene:phthalocyanine codeposited films deposited on heated substrate, Japan Journal of Applied Physics 43 (2004) 1014–1016.
[11] M. Vogel, J. Strotmann, B. Johnev, M. Luxsteiner, K. Fostiropoulos, Influence of nanoscale morphology in small molecule organic solar cells, Thin Solid Films 511–512 (2006) 367–370.
[12] S. Pfuetzner, C. Mickel, J. Jankowski, M. Hein, J. Meiss, C. Schuenemann, C. Elschner, A.A. Levin, B. Rellinghaus, K. Leo, The influence of substrate heating on morphology and layer growth in C60:ZnPc bulk heterojunction solar cells, Organic Electronics 12 (2011) 435–441.
[13] D. Wynands, M. Levichkova, M. Riede, M. Pfeiffer, P. Baeuerle, R. Rentenberger, P. Denner, K. Leo, Correlation between morphology and performance of low bandgap oligothiophene:C60 mixed heterojunctions in organic solar cells, Journal of Applied Physics 107 (2010) 014517.
[14] R. Fitzner, E. Reinold, A. Mishra, E. Mena-Osteritz, H. Ziehlke, C. Körner, K. Leo, M. Riede, M. Weil, O. Tsaryova, A. Weiß, C. Uhrich, M. Pfeiffer, P. Bäuerle, Dicyanovinyl-substituted oligothiophenes: structure–property relationships and application in vacuum-processed small molecule organic solar cells, Advanced Functional Materials 21 (2011) 897–910.
[15] J. Wagner, M. Gruber, A. Hinderhofer, A. Wilke, B. Bröker, J. Frisch, P. Amsalem, A. Vollmer, A. Opitz, N. Koch, F. Schreiber, W. Brütting, High fill factor and open circuit voltage in organic photovoltaic cells with diindenoperylene as donor material, Advanced Functional Materials 20 (2010) 4295–4303.
[16] G. Li, V. Shrotriya, J. Huang, Y. Yao, T. Moriarty, K. Emery, Y. Yang, High-efficiency solution processable polymer photovoltaic cells by self-organization of polymer blends, Nature Materials 4 (2005) 864–868.
[17] M. Sundberg, O. Inganäs, S. Stafstrom, G. Gustafsson, B. Sjogren, Optical absorption of poly(3-alkylthiophenes) at low temperatures, Solid State Communications 71 (1989) 435–439.
[18] N.I. Nijegorodov, W.S. Downey, The influence of planarity and rigidity on the absorption and fluorescence parameters and intersystem crossing rate constant in aromatic molecules, The Journal of Physical Chemistry 98 (1994) 5639–5643.
[19] P. Peumans, A. Yakimov, S.R. Forrest, Small molecular weight organic thin-film photodetectors and solar cells, Journal of Applied Physics 93 (2003) 3693.
[20] T. Offermans, P.A. van Hal, S.C.J. Meskers, M.M. Koetse, R.A.J. Janssen, Exciplex dynamics in a blend of pi-conjugated polymers with electron donating and accepting properties: MDMO-PPV and PCNEPV, Physical Review B (Condensed Matter and Materials Physics) 72 (2005) 45213.
[21] M. Hallermann, I. Kriegel, E. Da Como, J.M. Berger, E. von Hauff, J. Feldmann, Charge transfer excitons in polymer/fullerene blends: the role of morphology and polymer chain conformation, Advanced Functional Materials 19 (2009) 3662–3668.
[22] D. Veldman, O. İpek, S.C.J. Meskers, J. Sweelssen, M.M. Koetse, S.C. Veenstra, J.M. Kroon, S.S. van Bavel, J. Loos, R.A.J. Janssen, Compositional and electric field dependence of the dissociation of charge transfer excitons in alternating polyfluorene copolymer/fullerene blends, Journal of the American Chemical Society 130 (2008) 7721–7735.
[23] D. Veldman, S.C.J. Meskers, R.A.J. Janssen, The energy of charge-transfer states in electron donor–acceptor blends: insight into the energy losses in organic solar cells, Advanced Functional Materials 19 (2009) 1939–1948.
[24] C. Elschner, A.A. Levin, L. Wilde, J. Grenzer, C. Schroer, K. Leo, M. Riede, Determining the C_{60} molecule arrangement in thin films by means of X-ray diffraction, Journal of Applied Crystallography 44 (2011) 983–990.